ADVANCED MATERIALS
www.advmat.de

Unusual Pressure-Driven Phase Transformation and Band Renormalization in 2D vdW Hybrid Lead Halide Perovskites

Han Li, Ying Qin, Bohan Shan, Yuxia Shen, Fatih Ersan, Emmanuel Soignard, Can Ataca, and Sefaattin Tongay**

The application of high pressure allows control over the unit cell and interatomic spacing of materials without any need for new growth methods or processing while accessing their materials properties in situ. Under these extreme pressures, materials may assume new structural phases and reveal novel properties. Here, unusual phase transition and band renormalization effects in 2D van der Waals Ruddlesden–Popper hybrid lead halide perovskites, which have shown extraordinary optical properties and immense potential in light emission and conversion technologies, are reported. The results show that $(CH_3(CH_2)_3NH_3)_2(CH_3NH_3)Pb_2Br_7$ ($n = 2$) layers undergo two distinct phase transitions related to $PbBr_6$ octahedra, butylammonium (BA), and methylammonium (MA) molecule tilting motion that leads to rather unique/anomalous bandgap variation with pressure. In contrast, $(CH_3(CH_2)_3NH_3)PbBr_4$ ($n = 1$) lacks MA molecules and possesses only one pressure-induced phase transition related to $PbBr_6$ octahedra and BA tilting. In this range, the bandgap reduces monotonically, much similar to other inorganic semiconductors and display surprisingly large redshift from 3 to 2.4 eV. Together with theoretical calculations, this study offers unique insights into these pressure-induced changes and extends the understanding of these highly anisotropic layered soft organic perovskite materials under extreme conditions.

The organic–inorganic hybrid halide perovskite $CH_3NH_3PbX_3$ (X = Cl, Br, I) have gained significant scientific interest owing to their attractive properties and potential applications in solar cells and light emitting diodes.[1–6] Their superior optical properties, such as the long carrier diffusion length, largely tunable bandgap, and high optical absorption coefficients, together with their cost-effective production make them ideal materials for a variety of applications in energy conversion and optical sciences. Recent studies have shown that these bulk 3D hybrid halide perovskites can even be crystallized in layered form and have the general chemical formula of $(RNH_3)_2(CH_3NH_3)_{n-1}Pb_nX_{3n+1}$ where R is an alkyl or aromatic moiety,[7,8] X is a halide, and n is a variable that determines the number of metal-halide layers. In 2D perovskites, the constituent layers interact with each other through weak van der Waals (vdW) forces, and compared to their 3D counterpart, they offer even higher absorption coefficient, exotic exciton complexes, and larger exciton diffusion length.[9–11] Furthermore, these sheets can take a large amount of mechanical strain and can be isolated to single unit cell thickness to bring novel quantum effects arising from size confinement effects.[12,13]

Previously, a number of studies have studied the physical behavior of 3D hybrid halide perovskites under extreme hydrostatic pressures using diamond anvil cell (DAC) chamber design.[14–20] These pressure studies provide a powerful tool for changing interatomic distances and bond lengths on demand, and monitor structural, physical, or chemical properties and functionalities at finite pressures. Indeed DAC pressure studies on some of 3D hybrid halide materials to date have enabled new discoveries such as novel structural phase transitions and $PbBr_6$ octahedra distortions.[14,17] These pressure-induced effects are expected to be much different for 2D perovskites since the degree of interlayer interaction strength—which ultimately depends on the interlayer spacing and the hydrostatic pressure—ultimately dictates the overall properties and functionalities of 2D perovskites.[21] Despite their novel properties, the behavior of 2D perovskites under extreme pressures remains largely uncharted territory in the field and many fundamental questions are awaiting to be answered; *i*) how does the applied pressure influence the overall optical and structural characteristics of 2D layered perovskites? *ii*) Does the layer number n, in other words, the stacking layer number of the metal-halide octahedron, change pressure-dependent properties?

H. Li, Y. Qin, Dr. B. Shan, Dr. Y. Shen, Prof. S. Tongay
School for Engineering of Matter
Transport and Energy
Arizona State University
Tempe, AZ 85287, USA
E-mail: Sefaattin.tongay@asu.edu
Dr. F. Ersan
Department of Physics
Aydin Adnan Menderes University
Aydin 09100, Turkey
Dr. F. Ersan, Prof. C. Ataca
Department of Physics
University of Maryland Baltimore County
Baltimore, MD 21250, USA
E-mail: ataca@umbc.edu
Dr. E. Soignard
Eyring Materials Center
Arizona State University
Tempe, AZ 85287, USA
The ORCID identification number(s) for the author(s) of this article can be found under https://doi.org/10.1002/adma.201907364.

DOI: 10.1002/adma.201907364

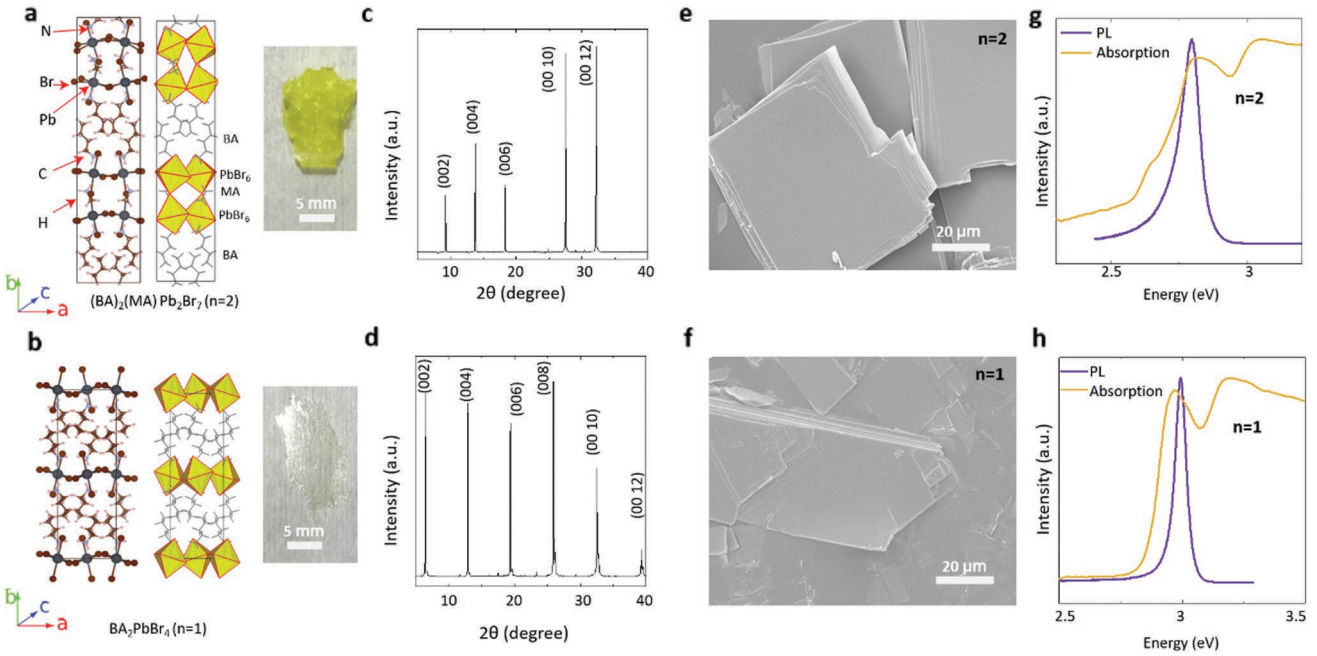

Figure 1. Characterization of 2D perovskite a) Crystal structure, schematic structure, and optical image of $(BA)_2MAPb_2Br_7$ ($n = 2$). b) Crystal structure, schematic structure, and optical image of $(BA)_2PbBr_4$ ($n = 1$). c) XRD of $(BA)_2MAPb_2Br_7$ ($n = 2$). d) XRD of $(BA)_2PbBr_4$ ($n = 1$). e) SEM image of $(BA)_2MAPb_2Br_7$ ($n = 2$). f) SEM image of $(BA)_2PbBr_4$ ($n = 1$). g) Photoluminescence (magenta trace) and UV–Vis absorption (yellow trace) of $(BA)_2MAPb_2Br_7$ ($n = 2$). h) Photoluminescence (magenta trace) and UV–Vis absorption (yellow trace) of $(BA)_2PbBr_4$ ($n = 1$).

In this work, we report on the high pressure studies in layered $n = 1$ and $n = 2$ 2D vdW Ruddlesden–Popper hybrid lead halide perovskite (RPP) $(BA)_2(MA)_{n-1}Pb_nBr_{3n+1}$ (n = layer number, BA is butylammonium, and MA is methylammonium).[8,22] Our studies were carried using diamond anvil cell chamber integrated with photoluminescence (PL), microabsorption, Raman spectroscopy systems which enables us to probe material behavior of RPP perovskites when the interlayer interactions are much enhanced at high pressures. These studies show that all RPP layered perovskites with different n values undergo dramatic phase transitions with applied pressure (0–15 GPa). Interestingly, however, the nature of the phase transition depends on the n value which suggests that the presence of MA building blocks heavily influences structural, vibrational, and optical response to applied pressure. The presented comprehensive pressure-dependent density functional theory (DFT) studies shed fundamental insights into the nature of the phase transitions as well as the pressure-dependent material properties.

2D layered perovskites used in this work are synthesized by established liquid crystallization method[23] (see methods for details) and the presentative crystal structures of $(BA)_2MAPb_2Br_7$ ($n = 2$) and $(BA)_2PbBr_4$ ($n = 1$) are schematically shown in **Figure 1**a,b. For the $n = 1$ case, $PbBr_6$ octahedrons are separated by only BA butylammonium without any MA methylammonium layers. Whereas, $n = 2$ layers consist of $PbBr_6$/MA layers separated by BA linkers. Measured X-ray diffraction (XRD) spectra and the peak positions for $n = 1$ and $n = 2$ closely agree with the previously reported data[24,25] as shown in Figure 1c,d. Scanning electron microscopy (SEM) images in Figure 1e,f clearly show the vdW layered nature of $n = 1$ and 2 RPP crystals, and these crystals can easily be exfoliated to thin-layers using standard mechanical exfoliation technique. Grown crystals and exfoliated sheets show strong PL emission signals which are located at 2.99 eV for $n = 1$ and 2.79 eV for $n = 2$ (Figure 1g,h magenta) in accord with the established values.[26,27] To extract out the E_g, we have used Tauc plot fitting and the measured absorption spectra were described well only with the direct gap expression $(\alpha h\nu)^2 = A(E - E_g)$ wherein α is absorption coefficient, $h\nu$ is photon energy, and A is a material-specific constant. The extrapolation results show that $n = 1$ exhibit E_g at 3.01 eV with a 2.88 eV located (defect) state and $n = 2$ with $E_g \approx 2.8$ eV and 2.68 eV located state as summarized in **Table 1**. Closer look at Figure 1g,h shows that the absorption maxima is located at higher energy values compared to PL emission energy which associated with the Stokes shift.[28]

To monitor the effects of applied pressure on the $(BA)_2MAPb_2Br_7$ ($n = 2$) sheets, ultra-thin sheets (lateral sizes ≈30 μm and ≈100 nm thickness) were loaded into our DAC chamber using sodium chloride (NaCl) as the pressure media. The rationale behind NaCl over ethanol–methanol liquid solution is to eliminate the detrimental effects of the

Table 1. Summary of experimental and theoretical bandgap values for 2D vdW Ruddlesden–Popper hybrid lead halide perovskite (RPP) $(BA)_2(MA)_{n-1}Pb_nBr_{3n+1}$ for $n = 1$ and 2.

Material	PL peak position [eV]	Calculated E_g [eV]	Absorption edge [eV]	Localized (Defect)
$(BA)_2MAPb_2Br_7$ ($n = 2$)	2.79	2.25	2.80	2.68
$(BA)_2PbBr_4$ ($n = 1$)	2.99	2.52	3.01	2.88

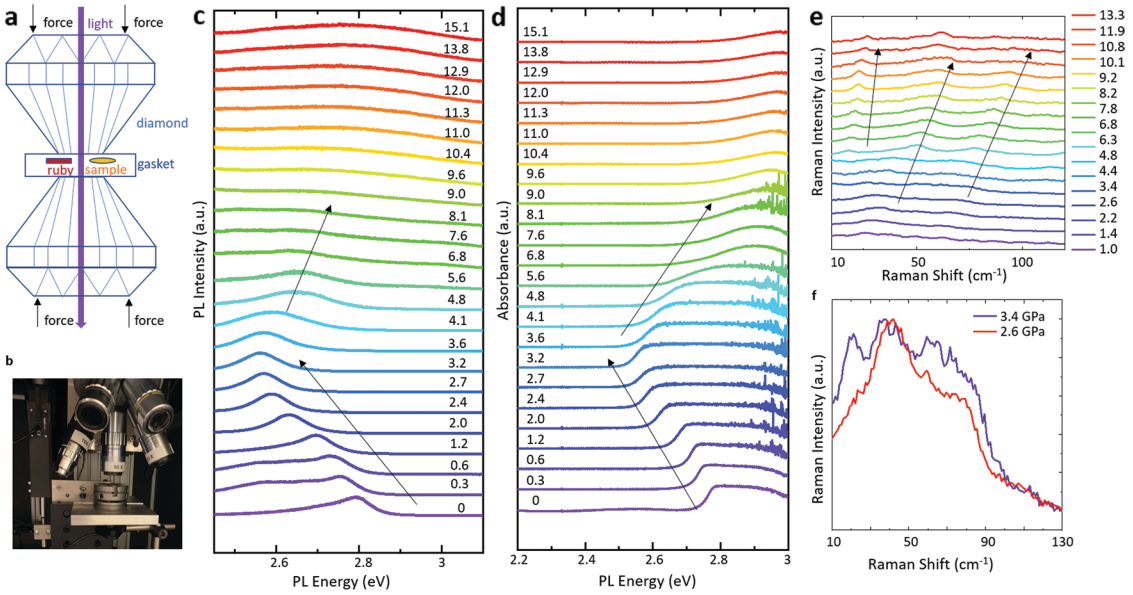

Figure 2. $(BA)_2MAPb_2Br_7$ ($n = 2$) phase transition at high pressure. a) Schematic diamond anvil cell. b) Diamond anvil cell under homemade Raman spectroscopy. c) Photoluminescence stacking with respect to pressure from 0 to 15.1 GPa. d) Micro absorption stacking plot from 0 to 15.1 GPa. e) Raman shift of perovskite from 1 to 13.3 GPa. f) Raman spectrum obtained at 2.6 and 3.4 GPa.

solution itself on $(BA)_2MAPb_2Br_7$ ($n = 2$) sheets. When pressure studies were performed using NaCl media, the material properties remained unchanged after full compression and decompression cycle without any permanent impact on the material properties. Unlike methanol–ethanol media, the use of NaCl also enabled us to apply uniaxial pressure[29] which is best suited for probing structural and physical changes related to interlayer distance and interaction strength. In our studies, we have applied pressures up to 15 GPa around which Raman, PL, and micro-absorption spectra became unmeasurably weak and the data analysis became unreliable. The pressure was measured using well-established ruby fluorescence technique[30] in close proximity to loaded RPP perovskite sheets (see schematic in **Figure 2**a), and the optical spectroscopy measurements were performed using our homemade setup integrated with the DAC chamber (Figure 2b).

In Figure 2c, we show the measured PL spectra of $(BA)_2MAPb_2Br_7$ ($n = 2$) sheets at a given pressure. From 0 to 3.4 GPa, the PL peak position redshifts from 2.79 to 2.56 eV at a rate of $dE_{gap}/dP \approx -67$ meV GPa^{-1} which is commonly observed behavior in traditional inorganic semiconductor materials. Interestingly, from 3.4 to 4.8 GPa PL peak position suddenly starts to blueshift from 2.56 to 2.64 eV with $dE_{gap}/dP \approx +54$ meV GPa^{-1}. We attribute this non-monotonic behavior to structural phase transition in 2D RPP perovskites. Another strong supporting evidence for phase transition comes from micro-Raman spectroscopy measurements that clearly show the phase transition and associated Raman spectra renormalization near the phase transition pressure regime (Figure 2e–g) by comparing micro-Raman spectra obtained at 2.6 and 3.4 GPa in Figure 2g. When $P = 2.6$ GPa, two prominent peaks appear at 30.8 and 66.7 cm^{-1}, but just slightly above 2.6 GPa Raman spectra renormalizes due to substantial structural changes and four vibrational modes appear at 8.7, 27.5. 53.7, and 74.0 cm^{-1}. Further evidence is also presented in Figure S1 (Supporting Information) where Raman modes stiffen and FWHM values suddenly differ around 3.4 GPa when phase transition takes place.

After the blueshifting regime from 3.4 to 4.8 GPa, the PL peak position starts to fluctuate from 4.8 to 8.1 GPa at around 2.62 eV as shown in **Figure 3**a (red circles) and after 9.0 GPa up to 15.1 GPa the bandgap continues to blueshift at a rate of $dE_{gap}/dP \approx 7$ meV GPa^{-1}. To better understand this non-monotonic pressure dependence, we have also carried out in situ micro-absorption spectroscopy measurements using our homemade micro-absorption system to access fundamental bandgap values at different pressures. Quantitatively results agree well with each other and PL and micro-absorption results are summarized in Figure 3a. Overall, the observed non-monotonic dE_{gap}/dP sign along with other spectroscopy measurements show the phase transition related effects and marks "the first observation of pressure-induced phase transition in 2D vdW hybrid halide perovskites."

From the theoretical perspective, the initial redshifting behavior is observed up to 9% compressive strain (or ≈3.5 Å reduction in b-axis lattice constant) and can be explained by closer orbital character analysis. The orbital character of VBM is mainly dominated by Br $4p_x$ and $4p_z$ orbitals and Pb 6s orbitals. In contrast, Pb $6p_z$ orbital solely dictates the CBM values (see Figure 3c). When the pressure is increased, the degeneracy of the VBM levels is lifted but this only results in negligible effect in comparison to experimentally observed changes in the bandgap values. But the energy level of Pb $6p_z$ orbitals for the CBM reduces by 0.5 eV under the applied compressive strain and leads to redshift in PL peak position (Figure 3b). While the absolute energy gap values differ from experimental ones, the overall calculated bandgap change with strain/pressure is in a good agreement with our experimental results. The difference in the absolute values can be easily attributed to the selected

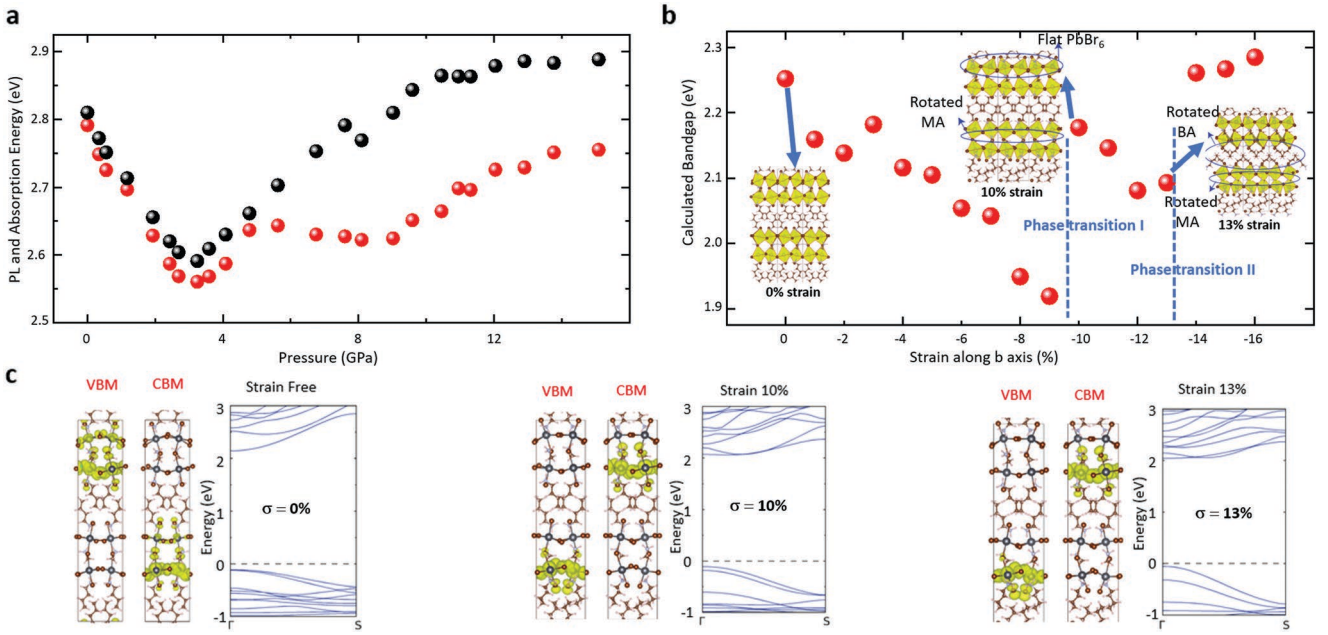

Figure 3. a) PL emission (red) and absorption edge (black) behavior under high pressure in $(BA)_2MAPb_2Br_7$. b) Calculated bandgap behavior with strain along b axis(stacking direction). c) VBM, CBM and band structure at 0%, 10%, and 13% strain.

generalized gradient approximation (GGA) functional of the DFT but does not influence the observed trends. If we compare the bond lengths between the Pb and Br atoms in *a*–*c* plane and the distance between successive Pb atoms in *b*-direction for strain-free and under strain (–9%) $(BA)_2MAPb_2Br_7$ ($n = 2$) sheets, we can see that the most reduction in distance has occurred at Pb-Br layers, which are separated by BA molecules. This reduced distance results in rotated BA molecules along the *b*-*a* axes and changes the Pb—Br bond lengths. Therefore, degeneracy in the electronic band structure decreases and the new energy levels arise yielding to the lower bandgap values.

While our theory studies show that the crystal matrix does not undergo any structural phase transition with *b*-axis strain from 0% to ≈9.5%, further increase in the compressive strain starts to make structural changes and leads to a blueshift in PL peak position (Figure 3b). High compressive strain beyond 10% first results in both tilting for the $PbBr_6$ octahedra and rotation MA molecules around the *c*-axis with respect to their original atomic positions in equilibrium structure. Because of these structural changes, the bandgap of the material starts to blueshift and span in that energy range up to 13% (see details in Figure S2, Supporting Information). Beyond 13% strain, BA molecules also start to rotate around their own axis marking another phase transition as labelled in Figure 3b. This phase transition is also accompanied by another large blueshift as shown in Figure 3b,c, and Figure S2 (Supporting Information). Here, we note that the theoretical strain values and experimentally attained pressure/strain values do not correspond one to one, but nevertheless overall experimental and theoretical bandgap variations show strong similarities with each other as shown in Figure 3a,b. More specifically, experimentally observed 0–3.4 GPa, 3.4–8.1 GPa, and 8.1–13 GPa ranges roughly correspond to 0–10%, 10–13%, and 13% to larger strain range.

To confirm the contributions of MA on phase transition and gain a more comprehensive understanding of layered perovskites, we investigated the pressure-dependent behavior of $(BA)_2PbBr_4$ ($n = 1$), in which MA is absent, with the same measurement condition of that in $(BA)_2MAPb_2Br_7$ ($n = 2$). As shown in **Figure 4**a, PL peak position only redshifts with increasing pressure from 3.00 eV at 0 GPa to 2.48 eV at 15.0 GPa. Overall bandgap change is quite monotonic with pressure and changes at $dE_{gap}/dP \approx -35$ meV GPa^{-1}. This value is much similar to other 2D inorganic excitonic semiconductors such as MoS_2, $MoSe_2$, and WSe_2 which is around –5 to –50 meV GPa^{-1}.[31–34] Similar changes can also be traced from micro-absorption measurements in Figure 4b. Our DFT results also support the experimentally observed redshift in the bandgap. The calculated bandgap reduces with pressure at a rate of –42 meV per % strain from 0% to –7% strain, and sharply decreased from –7% to –9% strain at a rate of –100 meV per % strain. Beyond these values, the bandgap change rate slows down to its original values ≈ –39 meV per % strain which is close to the rates observed at low pressure regime (Figure 4c). In contrast to $n = 2$ $(BA)_2MAPb_2Br_7$, for layered $n = 1$ $(BA)_2PbBr_4$ the all 4*p* orbitals give the same contribution to the VBM and hybridized with Pb 6s orbitals.

Similar to $n = 2$ case, the CBM is dominated by only Pb $6p_x$ orbitals and these orbitals contribution do not change with the increasing compressive strain ratio.

Furthermore, DFT structural relaxation studies show that significant structural phase transition takes place at around 8% strain. This strain value is also right around when the change in bandgap (dE_{gap}/dP) show a large difference (from –42 to –100 meV per % strain as marked with the blue dashed line in Figure 4c. A strong proof of structural phase transition comes from low-frequency Raman spectroscopy measurements. The Raman spectra undergo a large change at around 3.7 GPa as presented in Figure 4e (red dashed square)

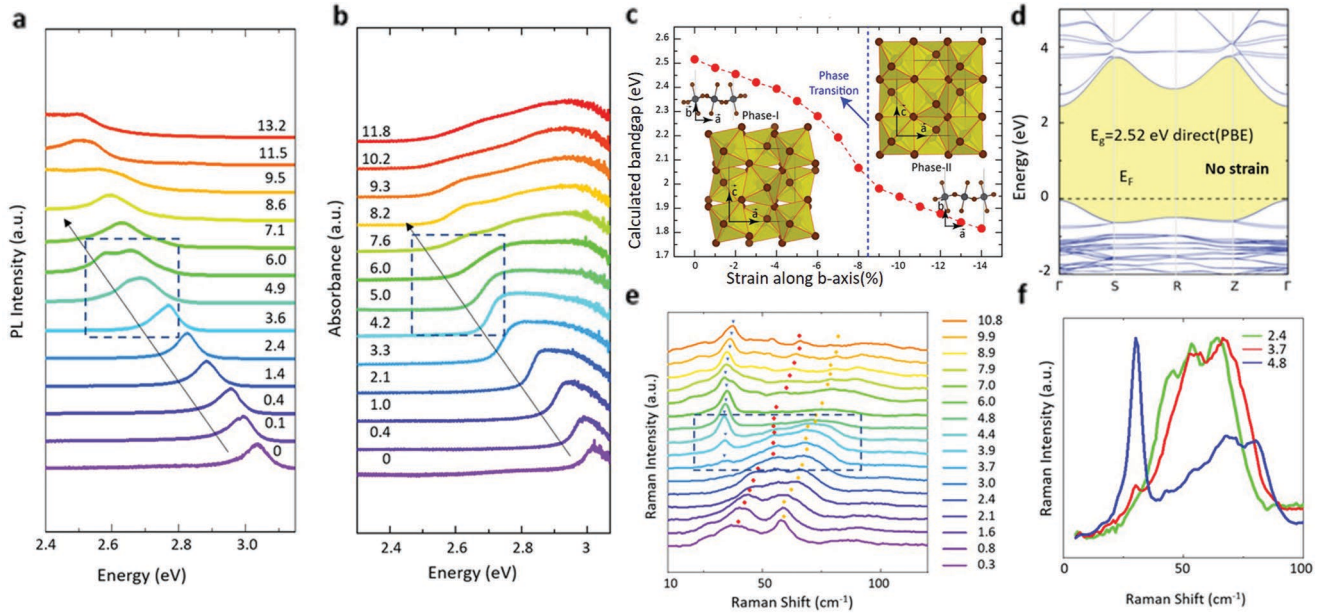

Figure 4. Characterization of $(BA)_2PbBr_4$ ($n = 1$) under high pressure a) PL stacking plot from 0 to 13 GPa. b) Micro absorption stacking plot from 0 to 12 GPa. c) Calculated bandgap change with strain along b axis. d) Band structure at 0% strain. e) Raman shift stacking plot of $(BA)_2PbBr_4$ ($n = 1$). f) Comparison of Raman spectrum at 2.4, 3.7, and 4.8 GPa.

and in zoom-in image in Figure 4f. We note that this change is reversible meaning upon releasing the DAC chamber pressure the Raman spectra goes back to its original form. A closer inspection into Raman spectra and change in Raman vibrational mode frequency (ω) with pressure ($d\omega/dP$) also show significant changes around the same pressure range (Figure S3, Supporting Information). Finally, we point out that PL spectra deviate from single Lorentzian fit (at 2.4 GPa) to stretched Gaussian ($P = 3.6$ GPa), broad peak ($P = 4.9$ GPa), eventually to double PL peak ($P = 6$ GPa) as can be seen in Figure 3a (red dashed square). Similar effects can also be observed for micro-absorption measurements in Figure 4b. These experimental and theoretical studies show that $(BA)_2PbBr_4$ $n = 1$ layers respond much differently to pressure when compared to $(BA)_2MAPb_2Br_7$ ($n = 2$) layers. The most notable difference is the monotonic bandgap reduction with pressure and a single phase transition presumably due to lack of MA molecules rotation related phase transition. Overall, these changes are fully reversible and during the entire course of the pressure cycle NaCl media does not react with the materials (Figures S4 and S5, Supporting Information).

In conclusion, we have demonstrated unusual pressure-driven phase transition, vibrational spectra, and band renormalization phenomena in 2D vdW Ruddlesden–Popper hybrid lead halide perovskite (RPP) $(BA)_2MAPb_2Br_7$ ($n = 2$) and $(BA)_2PbBr_4$ ($n = 1$). Results show that $(BA)_2MAPb_2Br_7$ ($n = 2$) layers undergo two distinct phase transitions related to $PbBr_6$ octahedra, BA, and MA molecule tilting motion as evidenced by comprehensive low-frequency Raman, absorption, and PL spectroscopy and DFT calculations. During back-to-back phase transitions, the bandgap changes non-monotonically with red- and blueshifts across the entire pressure range. In stark contrast to $n = 2$, $(BA)_2PbBr_4$ ($n = 1$) undergo only one phase transition related to $PbBr_6$ octahedra and BA tilting. Interestingly, the bandgap displays only monotonic redshift with pressure much similar to other traditional inorganic semiconductors. The underlying reasons for this unusual bandgap renormalization for $n = 2$ and substantial bandgap narrowing for $n = 1$ are in good agreement with band structure calculations and band-orbital. Overall results mark unusual phase transition behavior in 2D RPP materials, advance our understanding of their response under extreme conditions, and highlight the effect played by the chemistry on the overall phase transition behavior.

Experimental Section

Lead (II) oxide (PbO, 99.9%), hydrobromic acid (HBr, 48% w/w aq), hydro-phosphorous acid (H_3PO_2, 50% w/w aq), 1-butylammine (BA, 99%) are purchased from Alfa Aesar. Methylammonium bromide (MABr, 98%) is purchased from Sigma-Aldrich. All chemicals are used without further purification.

BA_2PbBr_4 ($n = 1$ material): 2.15 mL HBr and 0.425 mL H_3PO_2 are mixed together in a glass vial. 279 mg PbO (1.25 mmol) is added to the mixture. In a separate vial, 140 µL BA is added dropwise in 1.075 mL HBr in an ice bath to produce BABr solution. The content of both vials is then mixed and put in an autoclave for hydrothermal synthesis. The reaction temperature is raised in four hours till 110 °C, kept for 2 h, cooled to 50 °C in four hours, and further cooled to room temperature in 16 h.

$BA_2MAPb_2Br_7$ ($n = 2$ material): 2.15 mL HBr and 0.425 mL H_3PO_2 are mixed together in a glass vial. 279 mg PbO (1.25 mmol) and 70 mg MABr (0.625 mmol) is added in the mixture. In a separate vial, 87 µL BA is added dropwise in 1.075 mL HBr in an ice bath to produce BABr solution. The content of both vials is then mixed and put in an autoclave for hydrothermal synthesis. The reaction temperature is raised in four hours till 110 °C, kept for 2 hours, cooled to 50 °C in 4 h, and further cooled to room temperature in 16 h.

Our calculations are based on the first-principles plane wave method within density functional theory (DFT) using pseudopotentials supplied by Vienna Ab initio Simulation Package (VASP).[35] We approximate the exchange correlation functional with the Perdew Burke Ernzerhof flavor of the generalized gradient approximation (GGA).[36,37] vdW corrections included using D2-Grimme method.[38] We perform self-consistent field potential and ionic relaxation calculations for $(BA)_2(MA)_{n-1}PbnBr_{3n+1}$ (n = 1, 2) structures. In these calculations, the Brillouin zone (BZ) is sampled using (5 × 5 × 1) Monkhorst–Pack special k-points meshes.[39] We use a plane wave basis set with kinetic energy cutoff of 400.00 eV for the calculations. We set the energy convergence criterion between two successive iterations to be 10^{-5} eV, and kept the pressure less than 0.5 kB for the equilibrium structures. The Fermi surface was Gaussian smeared by 0.01 eV. The VESTA program was used to visualize atomic structures.[40]

Uniaxial pressure was applied to the sample through diamond anvil cell (DAC). Layered perovskites were placed in the gasket hole with 0.19 mm diameter. NaCl was used as pressure media to introduce uniaxial pressure. The fluorescence of ruby was used to determine the pressure in the DAC. PL spectra were measured with 355 nm UV laser and Raman spectra were measured with 532 nm green laser in backscattering configuration with 1200 mm^{-1} grating. The laser spot size was ≈1 µm and with power at the sample of 0.75 mW for Raman and 0.2µW for PL measurement.

UV–Vis absorption spectra were obtained by Lambda 950, Perkin-Elmer spectrophotometer. Deuterium and tungsten halogen lights were used as light sources for UV and visible range. 3 mm × 3 mm perovskite sample was attached to aperture. The spectrum range was from 250 nm to 800 nm, in step of 2 nm. Microabsorption spectra were obtained through a homemade spectrometer in a backscattering configuration. Tungsten light was used as light source. The spectrum range was from 350 nm to 750 nm, in step of 0.1 nm.

Materials were mechanically exfoliated on Si/SiO_2 substrates and gold was sputtered to increase sample conductivity. SEM images were collected using Amray 1910 with 10 kV accelerating voltage. X-ray diffraction is performed on a Siemens D5000 with Cu source.

Supporting Information

Supporting Information is available from the Wiley Online Library or from the author.

Acknowledgements

This work used the facilities within the Eyring Materials Center at Arizona State University supported in part by NNCI-ECCS-1542160. S.T. acknowledges funding from Army Research Office W911NF-18-1-0381, NSF CMMI 1933214, and NSF DMR 1552220, 1955889, and 1726213. C.A. acknowledges support from NSF DMR 1726213. The computational resources were provided by the UMBC High Performance Computing Facility (HPCF).

Conflict of Interest

The authors declare no conflict of interest.

Keywords

2D perovskites, band re-normalization, methylammonium molecule, pressure-driven phase transitions, stacking number *n*

Received: November 9, 2019
Revised: December 22, 2019
Published online: January 28, 2020

[1] N. Pellet, P. Gao, G. Gregori, T. Y. Yang, M. K. Nazeeruddin, J. Maier, M. Grätzel, *Angew. Chem., Int. Ed.* **2014**, *53*, 3151.
[2] O. Malinkiewicz, A. Yella, Y. H. Lee, G. M. Espallargas, M. Graetzel, M. K. Nazeeruddin, H. J. Bolink, *Nat. Photonics* **2013**, *8*, 128.
[3] J. H. Heo, S. H. Im, J. H. Noh, T. N. Mandal, C.-S. Lim, J. A. Chang, Y. H. Lee, H.-j. Kim, A. Sarkar, M. K. Nazeeruddin, M. Grätzel, S. I. Seok, *Nat. Photonics* **2013**, *7*, 486.
[4] S. T. Ha, X. Liu, Q. Zhang, D. Giovanni, T. C. Sum, Q. Xiong, *Adv. Opt. Mater.* **2014**, *2*, 838.
[5] R. Yang, R. Li, Y. Cao, Y. Wei, Y. Miao, W. L. Tan, X. Jiao, H. Chen, L. Zhang, Q. Chen, *Adv. Mater.* **2018**, *30*, 1804771.
[6] J. Byun, H. Cho, C. Wolf, M. Jang, A. Sadhanala, R. H. Friend, H. Yang, T. W. Lee, *Adv. Mater.* **2016**, *28*, 7515.
[7] Z. Wang, Q. Lin, F. P. Chmiel, N. Sakai, L. M. Herz, H. J. Snaith, *Nat. Energy* **2017**, *2*, 17135.
[8] Y. Chen, Y. Sun, J. Peng, J. Tang, K. Zheng, Z. Liang, *Adv. Mater.* **2018**, *30*, 1703487.
[9] L. M. Herz, *Annu. Rev. Phys. Chem.* **2016**, *67*, 65.
[10] M. B. Johnston, L. M. Herz, *Acc. Chem. Res.* **2015**, *49*, 146.
[11] S. De Wolf, J. Holovsky, S.-J. Moon, P. Löper, B. Niesen, M. Ledinsky, F.-J. Haug, J.-H. Yum, C. Ballif, *J. Phys. Chem. Lett.* **2014**, *5*, 1035.
[12] J. Even, L. Pedesseau, C. Katan, *ChemPhysChem* **2014**, *15*, 3733.
[13] J. A. Sichert, Y. Tong, N. Mutz, M. Vollmer, S. Fischer, K. Z. Milowska, R. García Cortadella, B. Nickel, C. Cardenas-Daw, J. K. Stolarczyk, *Nano Lett.* **2015**, *15*, 6521.
[14] L. Wang, K. Wang, B. Zou, *J. Phys. Chem. Lett.* **2016**, *7*, 2556.
[15] S. Jiang, Y. Fang, R. Li, H. Xiao, J. Crowley, C. Wang, T. J. White, W. A. Goddard III, Z. Wang, T. Baikie, *Angew. Chem., Int. Ed.* **2016**, *55*, 6540.
[16] M. Szafrański, A. Katrusiak, *J. Phys. Chem. Lett.* **2017**, *8*, 2496.
[17] P. Postorino, L. Malavasi, *MRS Bull.* **2017**, *42*, 718.
[18] X. Chen, H. Lu, Y. Yang, M. C. Beard, *J. Phys. Chem. Lett.* **2018**, *9*, 2595.
[19] J.-H. Lee, N. C. Bristowe, J. H. Lee, S.-H. Lee, P. D. Bristowe, A. K. Cheetham, H. M. Jang, *Chem. Mater.* **2016**, *28*, 4259.
[20] R. Zhang, W. Cai, T. Bi, N. Zarifi, T. Terpstra, C. Zhang, Z. V. Verdeny, E. Zurek, S. Deemyad, *J. Phys. Chem. Lett.* **2017**, *8*, 3457.
[21] G. Liu, J. Gong, L. Kong, R. D. Schaller, Q. Hu, Z. Liu, S. Yan, W. Yang, C. C. Stoumpos, M. G. Kanatzidis, *Proc. Natl. Acad. Sci. USA* **2018**, *115*, 8076.
[22] C. C. Stoumpos, D. H. Cao, D. J. Clark, J. Young, J. M. Rondinelli, J. I. Jang, J. T. Hupp, M. G. Kanatzidis, *Chem. Mater.* **2016**, *28*, 2852.
[23] J. Calabrese, N. Jones, R. Harlow, N. Herron, D. Thorn, Y. Wang, *J. Am. Chem. Soc.* **1991**, *113*, 2328.
[24] M. Jung, T. J. Shin, J. Seo, G. Kim, S. I. Seok, *Energy Environ. Sci.* **2018**, *11*, 2188.
[25] G. Feng, Y. Qin, C. Ran, L. Ji, L. Dong, W. Li, *APL Mater.* **2018**, *6*, 114201.
[26] L. Dou, A. B. Wong, Y. Yu, M. Lai, N. Kornienko, S. W. Eaton, A. Fu, C. G. Bischak, J. Ma, T. Ding, *Science* **2015**, *349*, 1518.
[27] N. R. Venkatesan, J. G. Labram, M. L. Chabinyc, *ACS Energy Lett.* **2018**, *3*, 380.
[28] K. Leng, I. Abdelwahab, I. Verzhbitskiy, M. Telychko, L. Chu, W. Fu, X. Chi, N. Guo, Z. Chen, Z. Chen, *Nat. Mater.* **2018**, *17*, 908.
[29] N. Tateiwa, Y. Haga, *Rev. Sci. Instrum.* **2009**, *80*, 123901.
[30] A. Dewaele, M. Torrent, P. Loubeyre, M. Mezouar, *Phys. Rev. B* **2008**, *78*, 104102.
[31] D. Lloyd, X. Liu, J. W. Christopher, L. Cantley, A. Wadehra, B. L. Kim, B. B. Goldberg, A. K. Swan, J. S. Bunch, *Nano Lett.* **2016**, *16*, 5836.

[32] X. Fu, F. Li, J.-F. Lin, Y. Gong, X. Huang, Y. Huang, H. Gao, Q. Zhou, T. Cui, *J. Phys. Chem. C* **2018**, *122*, 5820.
[33] H. Ehrenreich, *Phys. Rev.* **1960**, *120*, 1951.
[34] J.-S. Kim, R. Ahmad, T. Pandey, A. Rai, S. Feng, J. Yang, Z. Lin, M. Terrones, S. K. Banerjee, A. K. Singh, *2D Mater.* **2017**, *5*, 015008.
[35] G. Kresse, J. Furthmüller, *Phys. Rev. B* **1996**, *54*, 11169.
[36] P. E. Blöchl, *Phys. Rev. B* **1994**, *50*, 17953.
[37] J. P. Perdew, K. Burke, M. Ernzerhof, *Phys. Rev. Lett.* **1996**, *77*, 3865.
[38] S. Grimme, *J. Comput. Chem.* **2006**, *27*, 1787.
[39] H. J. Monkhorst, J. D. Pack, *Phys. Rev. B* **1976**, *13*, 5188.
[40] K. Momma, F. Izumi, *J. Appl. Crystallogr.* **2011**, *44*, 1272.